Gold Nanoparticles

DOI: 10.1002/anie.200603516

Site-Specific Recognition of Nanophase-Separated Surfaces of Amphiphilic Block Copolymers by Hydrophilic and Hydrophobic Gold Nanoparticles**

Shigeru Watanabe, Ryutaro Fujiwara, Masanori Hada, Yuka Okazaki, and Tomokazu Iyoda*

Ordered two and three-dimensional arrays of uniformly distributed nanoparticles are attractive for applications in nanoelectronics,[1] nanooptics,[2] and plasmonics.[3] Bottom-up fabrication techniques such as self-assembly and Langmuir–Blodgett techniques have been extensively explored. More recently, highly ordered nanoarrays have been successfully fabricated by a template method that uses natural nanoarchitectures such as DNA,[4,5] bacterial surface layer proteins,[6,7] ferritin,[8] chaperonin,[9] viruses,[10,11] and bacteriophages.[12] These methods provide attractive bottom-up fabrication schemes to produce regular nanoscale patterns; however, most natural templates require tedious handling and preparation. In this respect, artificial nanoarchitectures such as nanophase-separated block copolymers have distinctive advantages. In particular, diblock copolymer films that provide cylindrical nanodomains oriented perpendicular to the substrate are attractive because they produce templates and masks that are predicatable and controllable with nanoscale order. Recently, Iyoda and co-workers prepared amphiphilic diblock copolymers, PEO_m-*b*-$PMA(Az)_n$,[13] consisting of hydrophilic polyethylene oxide (PEO) and hydrophobic polymethacrylate with azobenzene-based liquid crystalline side-chains (PMA(Az)), which readily self-assemble into hexagonally packed PEO cylinders in a PMA(Az) matrix. At the surface, each PEO domain is in the form of a circular hollow surrounded by the PMA(Az) matrix. The periodic structure of PEO domains arranged with hexagonal symmetry is regularly tunable by changing the relative volume fractions of the copolymer components. However, to use such PEO_m-*b*-$PMA(Az)_n$ films as nanotemplates for the construction of periodic nanoparticle arrays, it is necessary to elucidate fundamental features of site-specific recognition processes on these nanophase-separated surfaces. Herein, we report the self-assembly of gold nanoparticles on a nanophase-separated PEO_m-*b*-$PMA(Az)_n$ film. The effects of the surface properties, concentration of gold nanoparticles, dipping time, and the composition of the dispersion medium on-site coverage and selectivity were investigated by a dip-coating method.

Amphiphilic block copolymers (PEO_m-*b*-$PMA(Az)_n$) were prepared by a well-controlled living polymerization of 11-[4-(4-butylphenylazo)phenoxy]undecyl methacrylate by using PEO macroinitiators.[13b] The nanophase-separated PEO_m-*b*-$PMA(Az)_n$ films were cast on a silicon wafer from 3 wt % toluene solution, followed by annealing at 110–140 °C for 24 h under vacuum. The AFM topography images obtained with the light tapping mode demonstrate that PEO_{114}-*b*-$PMA(Az)_{48}$, PEO_{272}-*b*-$PMA(Az)_{75}$, and PEO_{454}-*b*-$PMA(Az)_{152}$ provided a hexagonally packed cylinder morphology (Figure 1). Histograms show cylinder periods of (25.3 ± 1.9) nm for PEO_{114}-*b*-$PMA(Az)_{48}$, (40.6 ± 2.0) nm for PEO_{272}-*b*-$PMA(Az)_{75}$, and (45.2 ± 2.5) nm for PEO_{454}-*b*-$PMA(Az)_{152}$.

To investigate site-specific recognition of PEO and PMA(Az) domains on the film surface, two kind of gold nanoparticles with hydrophilic[14] (**1**) and hydrophobic[15] surfaces (**2**) were prepared (Scheme 1). When films of the nanophase-separated PEO_{272}-*b*-$PMA(Az)_{75}$ were dipped into a 0.1–0.25 wt % solution of **1** ($d = (2.35 \pm 0.35)$ nm, where d = mean diameter) in EtOH and of **2** ($d = (2.17 \pm 0.40)$ nm) in Et_2O for 10–60 s, the hydrophilic and hydrophobic gold nanoparticles **1** and **2** selectively assembled on the PEO and PMA(Az) domains, respectively (Figure 2a and b). The site selectivity (S_{PEO}) of gold nanoparticles assembled on the nanophase-separated surface was 100 % over a selected area of 400×400 nm^2 when the film was dipped in a 0.1 wt % solution of **1** in EtOH for 10 s. When this dipping time was increased to 60 s, this site coverage (θ_{PEO}) increased from 15 % to 25 %, whereas S_{PEO} decreased from 100 % to 61 %. Increasing the concentration of **1** to 0.25 wt % resulted in an even higher θ_{PEO} (32 %). Further increasing the nanoparticle concentration to 0.5 wt %, however, resulted in significant aggregation (Figure 2c). Concentrated nanoparticle solutions completely suppressed the template effect of the PEO_m-*b*-$PMA(Az)_n$ film as the interparticle interactions were much stronger than the van der Waals forces between the surface ligands and the PEO domains.[16]

Figure 3 shows atomic force microscopy (AFM) images of **1** and **2** deposited from dispersions in EtOH/Et_2O. From the 20 % Et_2O/EtOH dispersion, the hydrophilic gold nanoparticles **1** self-assembled on the hydrophilic PEO domains

[*] Prof. Dr. S. Watanabe, R. Fujiwara, M. Hada
Department of Material Science
Kochi University
Kochi 780-8520 (Japan)
Fax: (+81) 88-844-8359
E-mail: watanabe@cc.kochi-u.ac.jp
Y. Okazaki
Kochi Prefectural Industrial Technology
Kochi 781-5105 (Japan)
Prof. Dr. T. Iyoda
Chemical Resource Laboratory, Tokyo Institute of Technology
R1-25 4259, Nagatsuda, Midori Ku, Yokohama, 226-8503 (Japan)

[**] This work is supported by Core Research for Evolutional Science and Technology (CREST) of Japan Science and Technology Corporation (JST) and by a Special Research Grant for Green Science from Kochi University.

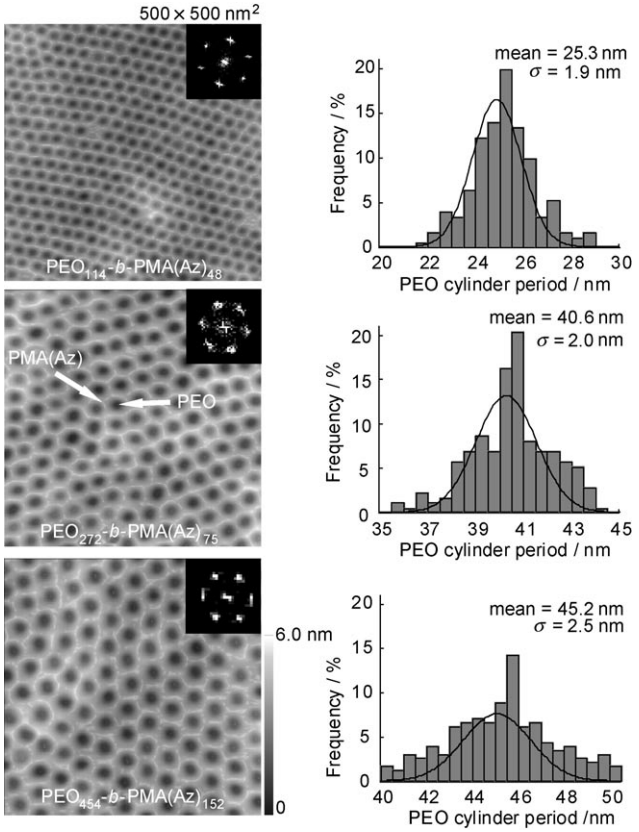

Figure 1. AFM topography images of a nanophase-separated surface on ultrathin PEO_m-*b*-$PMA(AZ)_n$ films prepared by spin-coating onto a silicon substrate and annealing at 140 °C for 24 h. The Fourier transformed patterns are shown on the right. The histograms were obtained by measuring more than 100 distances between the PEO cylinder centers.

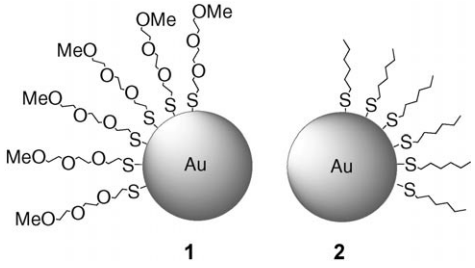

Scheme 1. Hydrophilic (**1**) and hydrophobic (**2**) gold nanoparticles.

(Figure 3a), whereas from the 40% Et_2O/EtOH dispersion, they were predominantly deposited on the hydrophobic PMA(Az) domains (Figure 3c). The hydrophilic gold nanoparticles **1** preferred binding to the hydrophobic sites with increasing Et_2O content. The hydrophobic gold nanoparticles **2** assembled on the hydrophobic PMA(Az) domains from the 20% EtOH/Et_2O dispersion, whereas they mostly deposited on the hydrophilic PEO domains from the 40% EtOH/Et_2O dispersion (Figures 3d–f). The preferred binding site of **2** changed from the hydrophobic domain to the hydrophilic domain with increasing EtOH content. Nanophase-separated block copolymer films are often subjected to solvent-induced

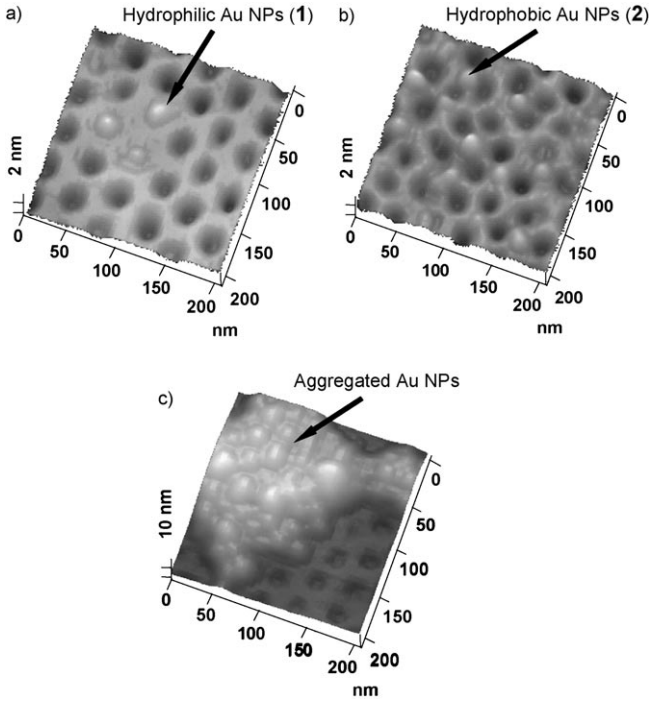

Figure 2. AFM topography images of hydrophilic and hydrophobic gold nanoparticles (NPs) **1** and **2** selectively organized on the PEO and PMA(Az) domains, respectively, of the nanophase-separated PEO_{272}-*b*-$PMA(AZ)_{75}$ film: a) [**1**] = 0.1 wt% (EtOH), dipping time = 10 s; b) [**2**] = 0.1 wt% (Et_2O); dipping time = 10 s. c) AFM topography image of aggregated gold nanoparticles upon dipping the film into a concentrated solution of gold nanoparticles **1** for a longer time: [**1**] = 0.5 wt% (EtOH), dipping time = 60 s.

topology changes.[17,18] When free PEO_m-*b*-$PMA(Az)_n$ films were exposed to EtOH and Et_2O for 60 s, swelling PEO and PMA(Az) domains, respectively, were observed by AFM. The solvent-induced inversion of the domain selectivity is due to domain-selective surface disorganization. EtOH disorders the PEO domain rather than the PMA(Az) domain, whereas Et_2O has the opposite effect. Gold nanoparticles preferentially assemble on the disordered active domain without their inherent selectivity.

Transfer of the gold nanoparticles from the template to a substrate is crucial for nanostructure fabrication (Figure 4a). Inexpensive and large-area vacuum ultraviolet (VUV) sources are highly desirable for industrial etching applications[19,20] Dry etching of the PEO_m-*b*-$PMA(Az)_n$ template was investigated by using VUV. The gold nanoparticles **1** that were assembled on the PEO_m-*b*-$PMA(Az)_n$ film were exposed to VUV radiation (172 nm) in the presence of O_2 at 25 °C for 1 h. FTIR spectra showed the time evolution of the loss of the C–H features at 2855 cm^{-1} and 2927 cm^{-1}, indicating decomposition of the PEO_m-*b*-$PMA(Az)_n$ template. An AFM image taken after this showed that spherical nanodots had been transferred to the underlying substrate (Figure 4c). The atomic composition of the nanodots was derived from X-ray photoelectron spectroscopy (XPS) studies. The Au $4f_{7/2}$ peak at 84.4 eV was in the range expected for Au^0 and was substantially lower than that of Au^I (85.1 eV)[21] and other oxidized Au compounds (Figure 4b). The mean center-to-

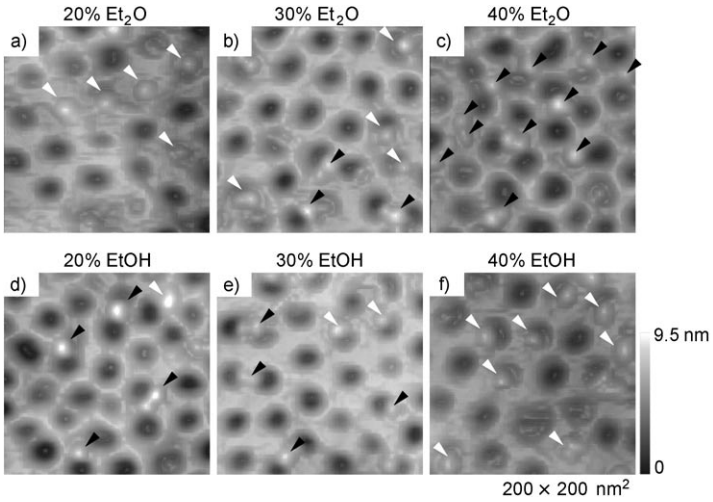

Figure 3. AFM topography images of hydrophilic (a–c) and hydrophobic gold nanoparticles (d–f) dip-coated on the nanophase-separated PEO_{272}-*b*-$PMA(AZ)_{75}$ film from a EtOH/Et_2O solution. Gold nanoparticles organized on the hydrophilic PEO domain (△) and on the hydrophobic PMA(Az) domain (▲).

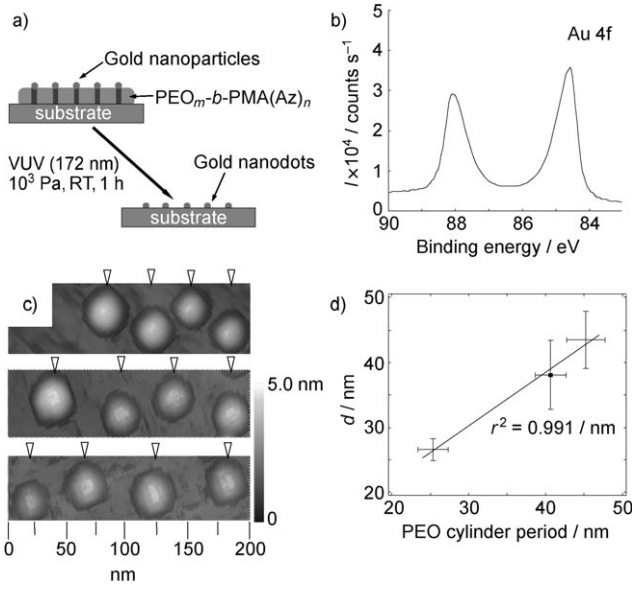

Figure 4. The gold nanoparticles **1** transferred to a silicon substrate by excimer VUV irradiation. a) Schematic illustration of transfer of gold nanoparticles from the template to a substrate. b) XPS spectrum of gold. c) AFM topography images. The block copolymers used as templates: PEO_{114}-*b*-$PMA(Az)_{48}$ (top), PEO_{272}-*b*-$PMA(Az)_{75}$ (middle), and PEO_{454}-*b*-$PMA(Az)_{152}$ (bottom). Open triangles show the lateral position of the gold nanodots. d) Plots of the nearest-neighbor distance between gold nanodots versus the PEO cylinder period of PEO_m-*b*-$PMA(Az)_n$ used as templates. More than 100 interdot distances in AFM images were averaged to determine the mean center-to-center distance between adjacent particles. The solid line represents a linear least-squares fit to the data. d = interdot distance.

center distances between the transferred gold nanodots correlated well with the PEO cylinder period of the PEO_m-*b*-$PMA(Az)_n$ used as the templates (Figure 4d).

In conclusion, we have demonstrated template-directed assembly of gold nanoparticles and the subsequent transfer of the arrayed nanoparticles to a substrate. The surface properties of the gold nanoparticles were the critical factor in this nanofabrication. Furthermore, solvent effects were significant enough to reverse the site selectivities of the particles. To further extend site coverage with high selectivity, gold nanoparticles should be modified by additional functional ligands providing electrostatic and hydrogen-bond interaction. VUV irradiation was effective in removing the PEO_m-*b*-$PMA(Az)_n$ template without destroying the regularity of the assembled nanoparticles. Such facile transfer is characteristic of soft (organic) templates but not of hard (inorganic) templates.

Experimental Section

Template-directed self-assembly of gold nanoparticles: A 3 wt % solution of PEO_m-*b*-$PMA(Az)_n$ in toluene was used for spin coating on a 1×1 cm^2 silicon substrate at 2000 rpm for 10 s. The spin-coated films were annealed at 110–140 °C for 24 h under vacuum to provide the nanophase-separated copolymer templates. The template-directed self-assembly of gold nanoparticles was performed by dipping the nanophase-separated copolymer templates into a 0.1–1.0 wt % suspension of gold nanoparticles in 0–100 % EtOH/Et_2O for 10–60 s at ambient temperature.

AFM measurements: AFM was performed in the tapping mode with a SPI3800N probe station and a SPA400 unit (Seiko Instruments Inc., Japan). Commercial silicon cantilever probes coated with Al, each with a nominal tip radius of less than 10 nm and a spring constant in the range of 2.5–10 N m^{-1}, were oscillated at their fundamental frequencies (between 100 and 200 kHz). Topographic (height) and phase images were recorded simultaneously at ambient conditions by using light tapping with a set-point ratio (A_{sp}/A_0) of 0.8–0.88, where A_0 and A_{sp} are the free oscillation and set-point amplitude, respectively. The scan field of view was set to 800×800 nm^2, 400×400 nm^2, and 200 nm $\times$ 200 nm^2 with a scan rate of 0.5–0.8 Hz and 512 scanning lines.

VUV irradiation: The nanoparticle-assembled film was placed in a vacuum chamber evacuated to 1.0×10^3 Pa by a rotary pump. The film was exposed to 172-nm VUV light generated from an excimer lamp (Ushio Inc., UER20–172 V, $\lambda = 172$ nm and 10 mW cm^{-2}) for 60 min.

XPS measurements: XPS was performed on an AXIS-HS spectrometer with a Mg anode unmonochromated X-ray source operated at a power of 60 W and 12 kV excitation voltage. The energy of the $Mg_{K\alpha}$ line was taken to be 1253.6 eV. The 180° hemispherical energy analyzer was operated in fixed-analyzer-transmission (FAT) mode. The pressure in the analysis chamber was approximately 10^{-8} Torr. Core level S 2p and Au 4f spectra were monitored. To compensate for surface charging effects, all binding energies were referenced to the C 1s neutral carbon peak at 284.3 eV.

Received: August 28, 2006
Published online: December 29, 2006

Keywords: diblock copolymers · gold · nanoparticles · surface chemistry · UV/Vis spectroscopy

[1] G. Schmid, B. Corain, *Eur. J. Inorg. Chem.* **2003**, 3081.

[2] C. P. Collier, R. J. Saykally, J. J. Shiang, S. E. Henrichs, J. R. Heath, *Science* **1997**, *277*, 1978.
[3] S. A. Maier, M. L. Brongersma, P. G. Kik, S. Meltzer, A. A. G. Requicha, H. A. Atwater, *Adv. Mater.* **2001**, *13*, 1501.
[4] N. C. Seeman, *Nature* **2003**, *421*, 427.
[5] S. Zhang, *Nat. Biotechnol.* **2003**, *21*, 1171.
[6] M. Mertig, R. Kirsch, W. Pompe, H. Engelhardt, *Eur. Phys. J. D* **1999**, *9*, 45.
[7] S. R. Hall, W. Shenton, H. Engelhardt, S. Mann, *ChemPhysChem* **2001**, *3*, 184.
[8] I. Yamashita, *Thin Solid Films* **2001**, *393*, 12.
[9] R. A. Mcmillan, C. D. Paavola, J. Howard, S. L. Chan, N. L. Zaluzec, J. D. Trent, *Nat. Mater.* **2002**, *1*, 247.
[10] Q. Wang, T. Lin, L. Tang, J. E. Johnson, *Angew. Chem.* **2002**, *114*, 477; *Angew. Chem. Int. Ed.* **2002**, *41*, 459.
[11] T. Douglass, M. Young, *Nature* **1998**, *393*, 152.
[12] S.-W. Lee, C. Mao, C. E. Flynn, A. M. Belcher, *Science* **2002**, *296*, 892.
[13] a) S. Y. Jung, T. Yamada, H. Yoshida, T. Iyoda, *J. Therm. Anal. Calorim.* **2005**, *81*, 563; b) Y. Tian, K. Watanabe, X. Kong, J. Abe, T. Iyoda, *Macromolecules* **2002**, *35*, 3739.
[14] M. Zheng, Z. Li, X. Huang, *Langmuir* **2004**, *20*, 4226.
[15] M. Brust, M. Walker, D. Bethell, D. J. Schiffrin, R. Whyman, *J. Chem. Soc. Chem. Commun.* **1994**, 801.
[16] D. Bargeman, F. Van Voorst Vader, *J. Electroanal. Chem.* **1972**, *37*, 45.
[17] T. Xu, J. Stevens, J. Villa, J. T. Goldbach, K. W. Guarini, C. T. Black, C. J. Hawker, T. P. Russell, *Adv. Funct. Mater.* **2003**, *13*, 698.
[18] K. Senshu, S. Yamashita, H. Mori, M. Ito, A. Hirao, S. Nakahama, *Langmuir* **1999**, *15*, 1754.
[19] V. Skurat, *Nucl. Instrum. Methods Phys. Res. Sect. B* **2003**, 208, 27.
[20] L. R. Allen, J. M. Grant, T. Nguyen, K. Valiev, L. Velikov, B. Meshman, *Solid State Technol.* **1995**, *38*, 77.
[21] S. K. Bhargava, F. Mohr, J. D. Gorman, *J. Organomet. Chem.* **2000**, *607*, 93.

